Computer-Aided Design 109 (2019) 33–48

Contents lists available at ScienceDirect

Computer-Aided Design

journal homepage: www.elsevier.com/locate/cad

# Overhang constraint for topology optimization of self-supported compliant mechanisms considering additive manufacturing☆

Alain Garaigordobil *, Rubén Ansola, Estrella Veguería, Igor Fernandez

*Department of Mechanical Engineering, Faculty of Engineering, University of the Basque Country, Alda, Urquijo s/n, 48013 Bilbao, Spain*

ARTICLE INFO

*Article history:*
Received 18 June 2018
Accepted 19 December 2018

*Keywords:*
Topology
Optimum design
Additive Manufacturing
Overhang
Compliant Mechanism

ABSTRACT

This work presents a computational procedure for direct integration of Topology Optimization and Additive Manufacturing (AM) technologies for compliant mechanisms design. Many topologically optimized geometries present manufacturing problems derived from the lack of self-supporting capacities and require sacrificial support material for 3D printing. The proposed strategy introduces a novel overhang constraint to control the amount of sacrificial support material required for additive manufacturing of compliant mechanisms. This overhang constraint is defined as the ratio between the value of self supported contours and the total amount of admissible and inadmissible contours, and is computed by an edge detection algorithm known as the Smallest Univalue Segment Assimilating Nucleus, that analyzes the geometry of the model for locating contours and computes their inclination and orientation. The proposed algorithm has been implemented as part of a software for computer aided design and several benchmark examples have been used to demonstrate the capacities of the approach.



## 1. Introduction

A mechanism is said to be compliant if its mobility entirely depends on the flexibility of its members. As a result, compliant mechanisms may be built from fewer parts, cutting the need for assembly processes to a minimum, while they also generate less friction, less wear, less backlash and reduce lubrication needs [1,2].

First methods regarding the design of compliant mechanisms were based on trial and error strategies, however, since the need for more direct and systematic methods and processes sprouted, new approaches have been proposed. These approximations are classified into lumped and distributed compliance approximations. Lumped compliant approaches convert rigid body mechanisms into partially compliant mechanisms by introducing little flexible pivots and rigid unions where needed, while a distributed compliant mechanism is obtained as the result of a topology optimization process for a particular design domain, boundary conditions and predefined performance specifications [3,4]. A distributed compliance approximation presents the main advantage of not requiring the predefinition of the number of connections nor the location of the flexible joints. In addition, the topology optimization problem can be based on flexibility-stiffness or functionality formulations. The latter can consider different objective functions, such as the Mechanical Advantage (MA), the Geometrical Advantage (GA) and the Work Ratio (WR), while the most common objective function for flexibility-stiffness formulations is the Mutual Potential Energy (MPE) that is equivalent to considering the output displacement or displacement of the output port. This work is focused on topology optimization with a flexibility-stiffness formulation.

Topology optimization is defined as a material lay-out problem, where the goal is to obtain the optimum material distribution along the design domain according to the predefined objective function, boundary conditions and constraint equations. The most extended topology optimization method in the synthesis of mechanisms is the Solid Isotropic Material with Penalization (SIMP). The method considers the properties of the elements as constant, and computes them as a function of the design variables. The property scaling function is defined as the product of the material property and the element density raised to a penalization factor [5,6]. A similar method is the Rational Approximation of Material Properties (RAMP) proposed in [7], however, there are many other different methods, as the Homogenization Method [8], heuristic methods as the Evolutionary Methods (ESO, AESO, BESO, SERA) [9–12], Level Set Method [13] and Topology derivatives [14] based methods, and some explicit alternatives as the very recent method of Moving Morphable Components (MMC) [15].

Topology optimization is a powerful designing tool with great free design capacities, and generally results in geometries far from intuitive. However, due to the complexity that most topologies are prone to present, there is a gap between the theoretical and practical uses of the topology optimization. Such gap is generated by the

☆ This paper has been recommended for acceptance by Charlie Wang.

* Corresponding author.
*E-mail addresses:* alain.garaigordobil@ehu.eus (A. Garaigordobil), ruben.ansola@ehu.eus (R. Ansola), estrella.vegueria@ehu.eus (E. Veguería), igor.fernandezdebustos@ehu.eus (I. Fernandez).

https://doi.org/10.1016/j.cad.2018.12.006

lag between manufacturing and design capacities, and involves the inability to manufacture geometries of great complexity. However, in recent years the development of the Additive Manufacturing (AM) technologies would have bridged this gap.

The AM and 3D printing technologies first appeared in the decade of 1980, and currently, a user can directly manufacture end-use parts, which certainly allows new design challenges (materials, shapes, internal structures, etc.) and favors the design freedom. Nevertheless, and although AM lacks the majority of the limitations present in classic manufacturing processes, there are still some technical aspects that should be catered in order to generate consistent geometries [16]. These issues include the minimum member size, the overhanging angles and the maximum overhanging distance [17,18]. Regarding the AM of topologically optimized components, the inclination of the overhanging members is a very important aspect since it is normally related with the geometric complexity of the part, and the capacity to deal with them depends on both, the process and the tool used. Nevertheless, there is a globally accepted agreement that considers the value of 45° as the theoretical minimum realizable overhang angle, measured from the base plate. This is supported by the bibliography [19]. Nevertheless, there are authors that propose values ranging from 20° to 45° [20], while others propose that not only the angle must be considered, but also the overhanging length. A member that violates the critical overhang angle condition is said to be not supported, and the parts that include unsupported regions are difficult, if not impossible, to manufacture. A general solution to such problems is the introduction of support structures during the manufacturing process. An alternative strategy is to ensure that the overhang angles are inside the admissible range of values, since that would mean that the part is totally self-supporting.

With the goal of bridging the gap between theoretical and practical applications of topology optimization, the idea of coupling design and manufacturing technologies (Topology Optimization and AM) sparked with many different approaches proposed since. Although there is no general classification of these approaches yet, the authors propose a listing according to the level of engagement of both technologies. Thus, the approaches are classified into three main groups. The first group encompasses the approaches where the ending design is directly sent to the 3D printing machine and scaffold structures are a viable alternative. The main advantage of these techniques is that the fabricated design is the optimum design itself, but only if the removal of all the support material is possible. On the other hand, the need for support material implies longer manufacturing time and higher overall costs. In order to reduce the volume of support material, some authors developed strategies where the optimum part orientation is sought [21], which is understood as the orientation inside the AM machine in which the required support material volume is the lowest. Nevertheless, changes in the part height and relative layer orientation may affect the manufacturing time and the mechanical properties of the manufactured part. J. Vanek, J. A. G. Galicia, and B. Benes [22] focused their efforts on the optimization of the scaffold structures and developed an strategy that, although it was constrained by the topology of the designed part, was able to reduce in certain amount the volume of the required support material. Other methods to reduce the volume of the sacrificial support material are proposed in [20,23,24].

The second group is formed by all the approaches that, for the sake of avoiding the need for sacrificial support material, introduce different intuition based modifications in the optimized topology. Once the topology optimization is over, the resulting design can or cannot be AM friendly, and in case it is not, and if the supports structures are not an option, these methods will introduce some handmade corrections of the geometry of the part. That is, the goal is to optimize the design with respect to the manufacturing process by making the geometry self-supporting [25]. With these techniques, the designer would generate a family of possible solutions, which are later analyzed by the Finite Element Method, and based on the results, the solution with the best response is chosen. However, nothing guarantees that the chosen design is close to the optimum.

Finally, the third and last group gathers all those methods where the design and manufacturing processes are totally integrated with each other. The design process will include specific additive manufacturing constraints within the topology optimization problem formulation. Such strategies will undoubtedly favor the design of completely self supported directly printable optimum parts. In the following some of the methods included in this last group are introduced.

Brackett [26] presented a strategy to solve the problem of designing completely self-supported structures by means of topology optimization. In that work, the idea of including an overhang constraint with the problem formulation is proposed along with a series of procedures to describe the overhang problem. However, the printed work did not include any example or numerical application. In [27] the authors proposed a wedge-shaped filter that, along with the topology optimization problem, allowed the design of self-supported structures. Recently, Langelaar [28,29] introduced a novel self-supported element filter which classifies the elements into printable and not-printable depending on the density of the elements below. The work proposed in [29] explores the possibility of optimum self-supported compliant mechanisms with the example of a compliant gripper, and stands as the first method addressing that field. Also very recently, Qian [30] developed a strategy based on the density gradient and the magnitude of the projected undercut perimeter, that allowed to control the formation of undercuts and the overhang angles during the optimization process.

Most of these works are based on the incorporation of filters that must be included in the traditional density-based topology optimization procedures, or on the introduction of some sort of local constraints [31]. Finally, there are some other works where the topology optimization problem is addressed from an explicit formulation, as it is for example in [32].

The particularities of the optimum design of self-supporting compliant mechanisms have not been addressed so far. Designing such devices can be cumbersome, and is not as straightforward as the design of self-supporting structures. The flexural pivots on compliant mechanisms are optimized so that the output is maximized/minimized and generally their shape is not free AM friendly. Therefore, if a completely self-supported compliant mechanism is desired, the flexural pivots will have to be corrected with the consequent performance penalization. This is defined as the compromise between performance and free additive manufacturability, and is widely explained in this paper.

This paper progresses in this line of work and presents a novel topology optimization approach for controlling the inclination of the members and designing optimal self-supporting compliant mechanisms. The proposed approach develops a novel global inequality constraint for the overhanging angle, which is included in the topology optimization problem formulation. The constraint refers to the ratio between supported and not supported "contours" instead of the traditional formulation of supported and unsupported "elements". This constraint can be easily added to the problem formulation as an additional inequality constraint along with the regular volume constraint for output displacement minimization/maximization problems, and coupled with traditional mathematical programming optimization algorithms, like the Method of Moving Asymptotes (MMA) [33]. The methodology used to identify and control the inclination of members is based on an edge detection algorithm developed in the field of digital image

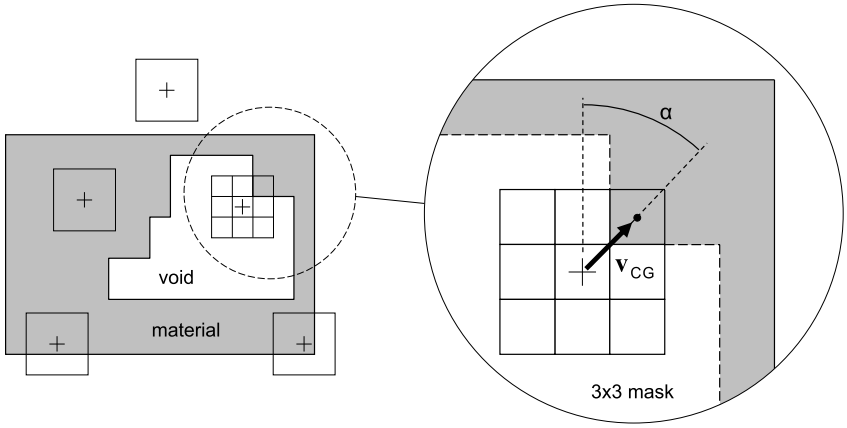


**Fig. 1.** Density gradient computation by means of the SUSAN operator.

processing known as the Smallest Univalue Segment Assimilating Nucleus (SUSAN). The procedure is implemented in a computer aided design (CAD) environment and allows the designer to specify not only any critical allowable overhang angle and printing direction, but also the tightness of the constraint through a control parameter that controls the ratio of self-supported contours. The capacities of this approach are demonstrated with extensive numerical examples and obtained results will show that the associated optimal output of self-supported parts can be close to that of the reference design.

Notice also that the AM of 2D compliant mechanisms is generally free of self-supporting problems as they are built on the horizontal plane. However, 3D mechanisms deal with such problems and are not straightforward to design. This work is a first approach to the design of self-supported compliant mechanisms that will derive in a future generalization to the 3D domain.

## 2. Boundary detection and overhang constraint

This section introduces the procedure used to detect contours and boundaries, along with the proposed overhang constraint. The procedure is based on an edge detection algorithm, able to recognize shapes and forms, and which gives information about the inclination of contours and boundaries. This will yield a constraint that describes the level of free AM of the part.

### 2.1. Contour evaluation algorithm

The overhang situation of any part is determined by the number, inclination and length of the overhanging members present in it, therefore, the first step to attempt to address the overhang problem is to develop an algorithm that can recognize shapes and detect edges and their inclination. For that reason, this work resorts to the field of digital image processing, and adapts an algorithm known as the Smallest Univalue Segment Assimilating Nucleus (SUSAN).

The SUSAN is used in digital image processing as a solid tool to detect image contours. It works by simultaneously sweeping the domain with a circular mask while analyzing the intensity gradient of the pixels covered by that mask. In each position of the mask the SUSAN operator counts the value that characterizes the similarities between each pixel of the image and its neighborhood [34]. Note that the positioning of the mask should allow its nucleus to match a pixel. The method has already proven its effectiveness and reliability in the field of digital image processing, it is fast when applied to optimization systems based on iterative evaluation of functions [35] and it is very easy to apply to 3D domains [36,37].

In this work, in order to adapt it to the design space, the original circular mask is converted to a $3 \times 3$ square mask, and the elemental density substitutes the pixel intensity. For every position of the mask, the density gradient ($\mathbf{v_{cg}}$) formed by the covered elements, its inclination and its direction can be computed (see Fig. 1).

The density gradient provides very important information considering that it joins the geometry center of the mask with its gravity center, and always points to the latter. Hence, it will always be normal to the detected contour. Besides, the module of the density gradient determines the existence of possible contours, with high values representing quick variations on the density field and closeness to a contour.

For a given position of the mask, $m$, the components of the gradient vector (${\boldsymbol{v}_{cg}}^m(x_{cg}, y_{cg})$) are computed as:

$$ {x_{cg}}^m = \frac{\int_A (x_i \cdot \rho_i) dA}{\int_A \rho_i dA} = \frac{\sum_{i=1}^{9} (x_i \cdot \rho_i)}{\sum_{i=1}^{9} \rho_i} \tag{1} $$

$$ {y_{cg}}^m = \frac{\int_A (y_i \cdot \rho_i) dA}{\int_A \rho_i dA} = \frac{\sum_{i=1}^{9} (y_i \cdot \rho_i)}{\sum_{i=1}^{9} \rho_i} \tag{2} $$

where $x_i$ and $y_i$ are the local coordinates of the centers of the elements inside the mask and $\rho_i$ is the element density. A regular mesh with square elements is considered so that the area $A_i$ of the elements can be removed from the equations [35].

The quality of each contour is known from the magnitude of the vector $\boldsymbol{v_{cg}}$. In the areas where the density field is close to uniform, that magnitude is small, and the mask is classified as a low quality boundary. Fig. 2 illustrates the contour analysis of a half inverter where white represents boundaries and black stands for homogeneous areas of void or material elements. The inverter mechanism converts an input force, applied at the input port, into a displacement at the output port in the opposite direction to the force.

Finally, and concerning edge detection, it must be noted that the original mesh is expanded with some dummy elements introduced in the background so that the outer boundaries of the design domain can be computed [38]. This dummy mesh consists of the regular mesh that defines the density distribution and four additional rows and columns of elements bordering the boundary of the design domain. The density of these dummy elements is taken as zero since they always correspond to the outside of the design region, except at the lower boundary, where in order to take into account the support that the plate of the printing machine provides, the density of the bottom dummy elements is taken as one. Obviously, this auxiliary mesh is for contour detection purposes only, and it is not considered during the finite element analysis of the structure.

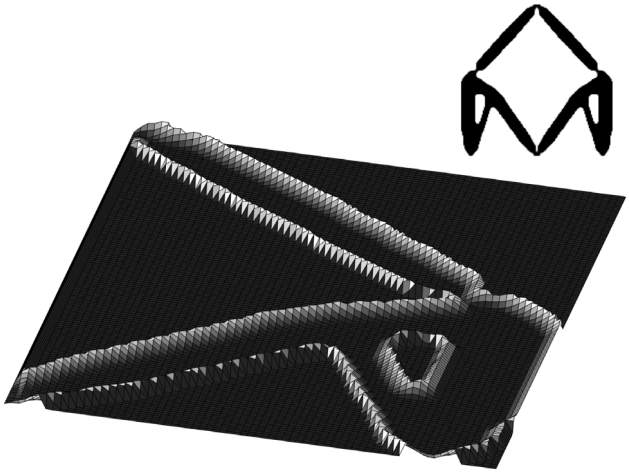

**Fig. 2.** Contour analysis of a half inverter. Physical representation of the density gradient.

### 2.2. Overhang constraint

The main objective of this work is to develop an effective and versatile overhang constraint to control the inclination of the members in topology optimization of compliant mechanism. Generally, the inclination of any member is described as the angle between the base plate and the down-facing contour, but this is similar to considering the angle between the material growing direction and a vector normal to the contour. The latter definition is more adequate for the better understanding of the method proposed in this work, therefore, the inclination of a member will be pictured likewise.

In Fig. 3, the overhanging angle is represented with $\alpha$ and its minimum allowable value is named as $\psi$. The material growing direction is a unitary vector ($\boldsymbol{r}$) defined by the designer, and normal to the plate. The minimum allowable inclination value is also designer chosen and as said before, there are many different values proposed in the bibliography according to the material and process used.

One way to determine whether a contour is self-supported, is to compare its inclination with the angle $\psi$. The latter behaves as a threshold parameter and according to the previous definition of the overhang angle, if $\alpha \geq \psi$, the member is said to be self-supported; otherwise, if $\alpha < \psi$, the member will need additional supporting material. Hence, in Fig. 3, for the same magnitude $x_{cg}$, there are one supported contour and one not-supported contour.

Nevertheless, this work rather than comparing angles it compares vertical projections, which simplifies the calculations and gives straightforward information. These values are depicted as $y_{cg}$ for the gradient vector and $y_\psi$ for an adjoint vector $\boldsymbol{v_\psi}(x_{cg}, y_\psi)$. Thus, in order to be self-supported, a contour must obey the inequation $y_{cg} \leq y_\psi$.

$$y_{cg} \leq y_\psi = \frac{|x_{cg}|}{\tan(\psi)} \tag{3}$$

$$\varphi(\boldsymbol{\rho}) = y_{cg} \cdot sin\psi - \left|x_{cg}\right| \cdot cos\psi \leq 0 \tag{4}$$

The right hand side of Eq. (3) represents the maximum allowable vertical projection of the gradient vector, previously denoted by $y_\psi$. Eq. (3) is normalized in Eq. (4), and the classification of whether the contours are supported or not supported is made according to this latter equation.

When the mask obeys $\varphi > 0$, the detected contour is said to be not supported and the value of $\varphi$ is stored in an array named as $\varphi^+$. On the contrary, if $\varphi \leq 0$ the contour is said to be supported and that value of $\varphi$ is stored in an array named as $\varphi^-$. It can be easily demonstrated that the normalized equation (4) is the cross product of vectors $\boldsymbol{v_{cg}}(x_{cg}, y_{cg})$ and $\boldsymbol{v_\psi}(x_{cg}, y_\psi)$, considering that both vectors are in the first quadrant, since the same behavior for vectors that are symmetric with respect to the vertical growing direction is desired. This paper however introduces a simplified version of that equation, rewriting it as shown in Eq. (5).

$$\hat{\varphi}_m(\boldsymbol{\rho}) = \sum_{i=1}^{9}(y_i \cdot \rho_i) sin\psi - \left|\sum_{i=1}^{9}(x_i \cdot \rho_i)\right| cos\psi = {q_y}^m sin\psi - |{q_x}^m| cos\psi \leq 0 \tag{5}$$

where $q_x$ and $q_y$ represent the static moments of the elements covered by mask.

Eq. (5), rewritten as $\varphi$ from now on, is thus used for classifying the contours into supported and not supported under the terms $\varphi^-$ and $\varphi^+$, respectively.

$$\varphi^+ = \sum_{m=1}^{M} \max(0, \varphi_m(\boldsymbol{\rho})) \tag{6}$$

$$\varphi^- = -\sum_{m=1}^{M} \min(0, \varphi_m(\boldsymbol{\rho})) \tag{7}$$

In Eqs. (6) and (7), the term M denotes the positions covered by the mask. With the previous classification done, the next step is to build the overhang constraint equation.

$$\hat{\phi}(\boldsymbol{\rho}) = \frac{\varphi^-(\boldsymbol{\rho})}{\varphi^-(\boldsymbol{\rho}) + \varphi^+(\boldsymbol{\rho})} \geq \phi_0 \tag{8}$$

The constraint equation (8) is defined as the ratio of the supported contours, which should be as close the unit as possible, being that the ideal situation where the number of not-supported contours is null ($\varphi^+ = 0$). Then, the mechanism is said to be self-supported and no sacrificial support material is needed. Eq. (8) is defined as the overhang ratio, and its value is of great importance in order to know if support free additive manufacturing is possible. However, comparing it the unit can be very aggressive for some topologies and result in designs with low structural meaning. Thus, rather than with the unit, the overhang ratio is compared with a tunable control parameter ($\phi_0$). As it will be demonstrated in Section 5, the value chosen for $\phi_0$ has a strong influence over the resulting topology and although there is not a standard value, the numerical experiments have shown that a control parameter of 0.97 results in adequate designs in most of the cases.

## 3. Density filtering and Heaviside projection

A common problem in topology optimization of continuum domains is the occurrence of checkerboard patterns, or regions of alternating solid and void elements, in the final solution. This phenomenon of alternating presence of solid and void elements ordered in a checkerboard like pattern makes the interpretation of optimal material distribution and geometric extraction for manufacturing difficult. Diaz and Sigmund [39] and Jog and Haber [40] showed that checkerboards are not optimal but rather result from numerical instabilities. A large amount of literature exists on preventing checkerboards patterns and mesh dependence. Popular approaches are to restrict the design space placing a constraint on the total perimeter of the structure so that solution exists for the original continuum problem [41] or to filter the values of sensitivities [42], which have been used extensively in a significant amount of works. In this work we will adopt a Heaviside projection method [43] since density filters have demonstrated to be more robust than sensitivity filtering schemes. The method first obtains

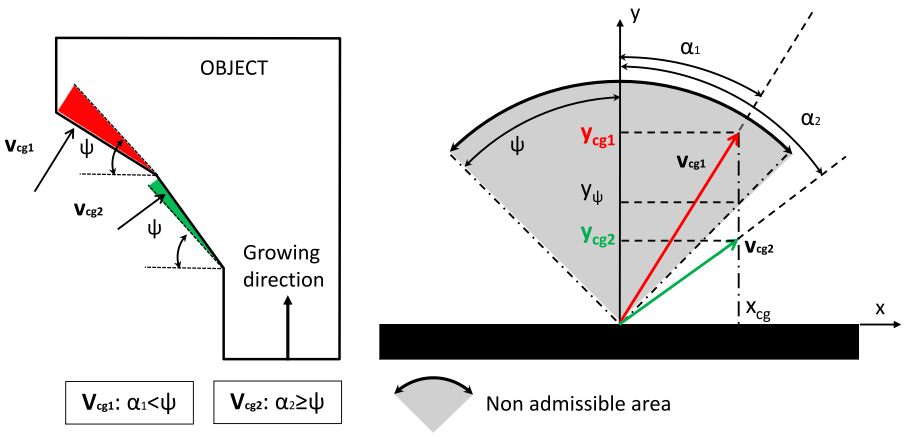


**Fig. 3.** Feasible area for the gradient vector.

an intermediate field of filtered design variables $\hat{\boldsymbol{\rho}}$ using a weighted average function (Eq. (9)).

$$\widehat{\rho_e} = \frac{\sum_{i \in S_e} \omega_i \cdot \rho_i}{\sum_{i \in S_e} \omega_i} \tag{9}$$

where $\omega_i$ is the weight factor, $S_e$ is the set of $i$ elements in the domain of influence of element $e$, that is, the set where the center-to-center distance to element $e$ is smaller than the filter radius $r_{min}$:

$$\omega_i = \max(0, r_{min} - |dist\ (e, i)|) \tag{10}$$

The smoothing operation above limits the space of possible designs and solves the mesh dependency problem. However, the smoothness of the designs also implies gray transition zones at the interface between material and void phases [44]. In order to avoid these gray zones, a projection step is added to the density filter where intermediate densities are projected by means of a regularized Heaviside function. In this work a continuous approximation of the Heaviside function based on the hyperbolic tangent function is used [45], where the values of $\hat{\rho}_e$ below $T$ are projected to 0 and the values above are projected to 1:

$$\overline{\rho_e} = \frac{\tanh\left(\beta \cdot T\right) + \tanh(\beta \cdot (\widehat{\rho_e} - T))}{\tanh\left(\beta \cdot T\right) + \tanh(\beta \cdot (1 - T))} \tag{11}$$

$\beta$ is a scaling parameter which controls the steepness of the continuous approximation of the Heaviside function and $T$ is the threshold parameter of the Heaviside function. The projected densities $\overline{\rho}_e$ are referred to as the physical densities and will substitute the regular density design variables; therefore, we will always present the filtered and projected density field $\overline{\rho}_e$ rather than the original density field $\rho_e$ as the solution to the optimization problem. Similarly, the objective and constraint functions will be computed using physical densities, provided that the variable $\rho_e$ is replaced with $\overline{\rho}_e$. It must be noted, that the sensitivities in the topology optimization problem become increasingly ill conditioned for high values of the parameter $\beta$ and a continuation scheme on the parameter $\beta$ is usually necessary during the optimization process. When working with large values of $\beta$ using the default MMA approach as we do in this investigation, the sharpness of that approximation to the step function may generate aggressive oscillations. Therefore, there are some adjustments that should be considered when a continuation scheme is applied, since there is iteration from which $\beta$ is great enough to generate oscillations. The required parameter adjustments can be found in [46], which basically consist in modifying the distance of the asymptotes from the current point in terms of the parameter $\beta$. Also, according to [46] a continuation scheme is introduced for the penalization parameter $p$. Initial values of $\beta = 5$ and $p = 3$, and increments of 5 and 2 respectively, have demonstrated to give solid results. Additionally, the maximum values reached by these parameters are 25 and 11 respectively.

## 4. Problem statement and sensitivity analysis

The topology optimization problem presented on this work is based on flexibility-stiffness formulations. It stands as the minimization of the displacement of the output port, and along with the regular volume constraint, a global overhang constraint is introduced in order to control and minimize the use of scaffold structures needed during the additive manufacturing process. Considering a linear model, the problem stands as,

$$\text{min:} \quad c(\overline{\boldsymbol{\rho}}) = u_{out} \tag{12}$$

$$\text{s.t.:} \quad \mathbf{K} \cdot \mathbf{U} = \mathbf{F} \tag{13}$$

$$V(\overline{\boldsymbol{\rho}}) \leq V_o \tag{14}$$

$$\phi(\overline{\boldsymbol{\rho}}) \geq \phi_o \tag{15}$$

$$0 < E_{min} \leq E_e \leq E_0 \tag{16}$$

$$u_{out} = \mathbf{l}^t \cdot \mathbf{U} \tag{17}$$

where $u_{out}$ is the displacement of the output port, $\boldsymbol{K}$ is the global stiffness matrix, $\boldsymbol{U}$ is the displacement vector and $\boldsymbol{F}$ the vector with the applied external force. $V(\overline{\boldsymbol{\rho}})$ and $V_0$ are the volume of the component and the objective volume respectively. Finally, $\phi(\boldsymbol{\rho})$ is the overhang constraint that corresponds to the ratio of printable contours, and $\boldsymbol{l}$ is a vector whose only non-zero component is the one corresponding to the degree of freedom of the output port, and that value is the unit.

The approximations of the properties of the elements are left to the SIMP method, which penalizes the intermediate densities with a penalization factor $p$. Each element is assigned a density value and its Young's modulus is scaled with the density-stiffness equation (18).

$$E_e\left(\overline{\rho}_e\right) = E_{min} + (E_0 - E_{min}) \cdot \overline{\rho_e}^p(\rho_e) \tag{18}$$

$E_0$ is the Young's modulus of the solid isotropic material and $E_{min}$ the corresponding Young's modulus of the void phase that is generally considered as $E_{min} = 10^{-9}$.

In order to compute the derivatives of any function $f(\overline{\boldsymbol{\rho}})$ involved in the problem with respect to the density of each element, and considering that filtering and projection operations are applied, the chain rule is applied.

$$\frac{\partial f(\overline{\boldsymbol{\rho}})}{\partial \rho_e} = \frac{\partial f(\overline{\boldsymbol{\rho}})}{\partial \overline{\rho}_e} \cdot \frac{\partial \overline{\rho}_e}{\partial \hat{\rho}_e} \cdot \frac{\partial \hat{\rho}_e}{\partial \rho_e} \tag{19}$$

The second and third terms on the right side of the equation can be obtained for any $f(\overline{\boldsymbol{\rho}})$ function as the direct derivatives of Eqs. (9) and (11).

$$\frac{\partial \overline{\rho}_e}{\partial \hat{\rho}_e} = \frac{\beta[1 - \tanh^2(\beta \cdot (\widehat{\rho_e} - T))]}{\tanh\left(\beta \cdot T\right) + \tanh(\beta \cdot (1 - T))} \tag{20}$$

$$\frac{\partial \hat{\rho}_e}{\partial \rho_e} = \frac{\omega_i}{\sum_{i \in S_e} \omega_i} \tag{21}$$

The derivative of the first term on the right hand side of Eq. (19) will vary depending on the nature of the function $f(\overline{\boldsymbol{\rho}})$ considered in each case. Considering the objective function, it is derived using the adjoint method [47].

$$\frac{\partial u_{out}(\overline{\boldsymbol{\rho}})}{\partial \overline{\rho}_e} = \boldsymbol{\lambda}^t \cdot \frac{\partial \mathbf{K}}{\partial \overline{\rho}_e} \cdot \mathbf{U} \tag{22}$$

$$\boldsymbol{\lambda}^t \cdot \mathbf{K} = -\mathbf{I}^t \tag{23}$$

where $\lambda$ is the vector that contains the Lagrangian multipliers obtained with Eq. (23).

The derivatives of the volume constraint equation with respect to the projected densities for substitution in the chain rule of Eq. (19) are obtained by:

$$\frac{\partial V(\overline{\boldsymbol{\rho}})}{\partial \overline{\rho}_e} = v_e \tag{24}$$

where $v_e$ represents the volume of finite element $e$. Finally, only the sensitivity calculation with respect to $\overline{\rho}_e$ of the projection restriction function remains. First thing is to normalize the inequality constraint shown in Eq. (8).

$$\phi\left(\overline{\boldsymbol{\rho}}\right) = \frac{\varphi^-\left(\overline{\boldsymbol{\rho}}\right) + \varphi^+(\overline{\boldsymbol{\rho}})}{\varphi^-\left(\overline{\boldsymbol{\rho}}\right)}\phi_0 - 1 \leq 0 \tag{25}$$

Taking derivatives in Eq. (25) and omitting density dependence for simplicity,

$$\frac{\partial \phi\left(\rho\right)}{\partial \overline{\rho}_e} = \phi_0 \cdot \frac{\frac{\partial \varphi^+}{\partial \overline{\rho}_e} \cdot \varphi^- - \frac{\partial \varphi^-}{\partial \overline{\rho}_e} \cdot \varphi^-}{(\varphi^-)^2} \tag{26}$$

The sensitivities of the supported and not-supported contours, $\varphi^-$ and $\varphi^+$, can be calculated taking derivatives of Eqs. (6) and (7):

$$\frac{\partial \varphi^+}{\partial \overline{\rho}_e} = \sum_{m=1}^{M} \begin{cases} 0 & \varphi_m \leq 0 \\ \dfrac{\partial \varphi_m}{\partial \overline{\rho}_e} & \varphi_m > 0 \end{cases} \tag{27}$$

$$\frac{\partial \varphi^-}{\partial \overline{\rho}_e} = \sum_{m=1}^{M} \begin{cases} \dfrac{-\partial \varphi_m}{\partial \overline{\rho}_e} & \varphi_m \leq 0 \\ 0 & \varphi_m > 0 \end{cases} \tag{28}$$

Finally, it is necessary to compute the derivatives of the contour values at each position of the mask,$\varphi_m$, for substitution in Eqs. (27) and (28). Recalling Eq. (5) for contour evaluation, the derivatives can be obtained with the following expression:

$$\frac{\partial \varphi_m}{\partial \overline{\rho}_e} = \frac{\partial {q_y}^m}{\partial \overline{\rho}_e} \cdot \sin\psi - \frac{{q_x}^m}{|{q_x}^m|} \cdot \frac{\partial {q_x}^m}{\partial \overline{\rho}_e} \cdot \cos\psi \tag{29}$$

The derivatives of the static moments can be easily obtained as,

$$\frac{\partial {q_x}^m}{\partial \overline{\rho}_e} = {x_e}^m \tag{30}$$

$$\frac{\partial {q_y}^m}{\partial \overline{\rho}_e} = {y_e}^m \tag{31}$$

Then, recalling (29),

$$\frac{\partial \varphi_m}{\partial \overline{\rho}_e} = {y_e}^m \cdot \sin\psi - \frac{{q_x}^m}{|{q_x}^m|} \cdot {x_e}^m \cdot \cos\psi \tag{32}$$

Once the sensitivities of the objective functions and constraints are calculated, the optimization problem is formulated and solved using the MMA. There is still the definition of the design domain and the basic parameters of the optimization problem (loads, boundary conditions etc.). The volume restriction, as well as, the growing direction and the maximum overhang angle are defined at this point too.

After variables are smoothed and projected in order to obtain the physical density field, the contour evaluation loop starts. The gradients for all the different mask positions are calculated and the overhang constraint value is obtained. Then, for the same material distribution, the volume and output displacement are computed by the finite element method. Finally, sensitivity analysis is performed and densities are updated by means of the MMA. Every 50 iterations the parameters $p$ and $\beta$ are updated by means of the continuation scheme until they reach their maximum values. Once these values are reached, the process will end when a marginal update of the design variable is achieved with respect to the last design, where marginal means $10^{-4}$. Once the optimization problem is over, a 3D CAD model is built based on the optimal material distribution that is later converted to a.STL file and finally sent it to the 3D printing machine.

## 5. Influence of the control parameter and effect over the hinges. On the compromise between free AM and optimum performance

This section focuses on studying the hinges and the effects of the parameters controlling the inclination of the members over them, paying special attention to the control parameter.

With the control parameter the designer can adjust and control the minimum amount of well supported masks as it is shown in Fig. 4. That figure shows the theoretical minimum allowable ratio of the supported contours (dotted line) for different values of the control parameter. In practice however, there is a natural ratio of self-supported elements for every component ($\phi_{natural}$), defined as the value showed by the non-constrained result. For any value of $\phi_0$ below $\phi_{natural}$, the material will always be distributed as in the non-constrained material layout problem describing the black line behavior.

Effectively, the natural overhang ratio is unique for every material layout and every overhang angle and therefore is function of the parameters that govern the design problem. Its value is representative of the overhang situation, and performs as the threshold that defines whether the overhang constraint is acting or not.

High threshold values mean that most of the contours are self-supported for the given angle, while low values denote that most of the contours lack support. However, its value is only representative of the overhang situation of the unconstrained optimum design and it is not imperative to know it to solve the topology optimization problem of self-supported structures or compliant mechanisms. Nevertheless, knowing the natural overhang ratio may be interesting in order to know if the overhang constraint will be acting or not, and in case it is in which level it is acting.

Fig. 4 shows an example of how the definition of the control parameter affects the behavior of the overhang constraint and the optimization problem when the natural overhang ratio is 0.6. The dotted line denotes the minimum allowable overhang ratio values, and it is appreciable that for any value of $\phi_0$ below $\phi_{natural}$, the material will always be distributed as in the non-constrained material layout problem.

The effect of the control parameter over structures is very straightforward and can be resumed as in the previous lines, for mechanisms however, this is more complex and requires further attention. The following lines introduce the reason for that increased complexity, and analyze how designers can build an adequate strategy taking advantage of the control parameter, and the flexible overhang constraint.

### 5.1. Effects of the control parameter over the hinges

A hinge or point flexure (flexure pivot) is defined as a one-node linkage formed joint with a similar behavior to a revolute joint in

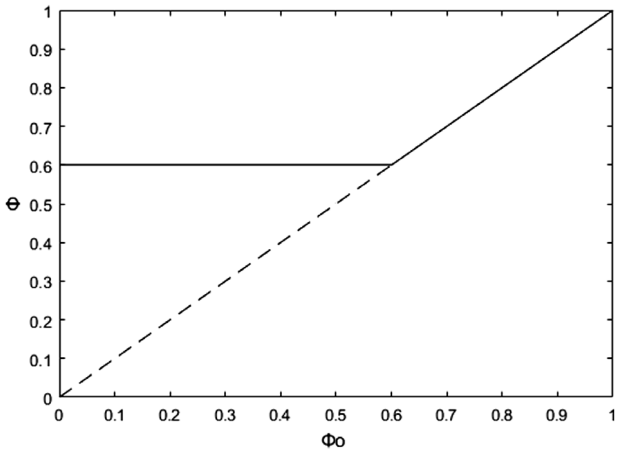


**Fig. 4.** Evolution of the level of self-support for different values of the control parameter and considering a $\phi_{natural}$ of 0.6: theoretical and real minima.

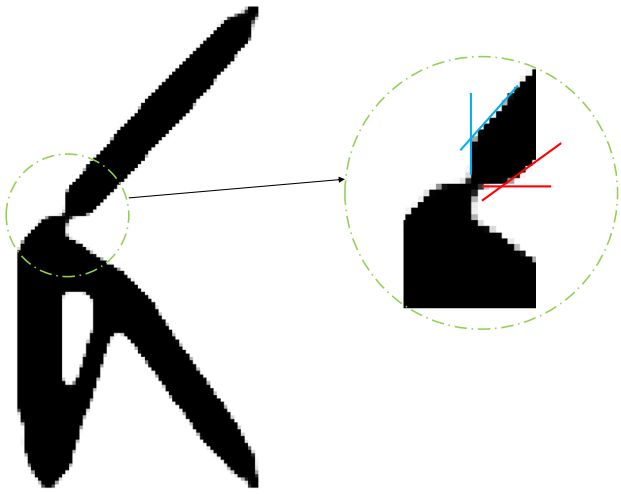

**Fig. 5.** Boundary slopes of a hinge.

rigid-body linkages [48]. That one node joint is nonetheless mechanically unrealistic and impossible to manufacture, so avoiding the formation of these point flexures is been a worry for designers since the topology optimization techniques were considered in the synthesis of compliant mechanisms. For flexibility-stiffness formulations, that simultaneously maximized the output displacement and the overall stiffness, the theoretically optimum approach was a rigid-body linkage with revolute joints, since that would generate large output motion for a given force while strain energy is kept to minimum (zero). Practice is very different though, with a range of motion limited by the lumped compliance that leads to high local stresses at hinges [49] that in reality would approach infinity in the sharpest, causing the breakage of the structure. The resulting are not purely compliant bodies on account of the tendency to form what amounts to almost moment-free one node connected hinges [47]. In literature one can find many different approaches to obtain a problem formulation that leads to hinge-free distributed compliant mechanisms [44,50,51].

An additional way to tackle the hinge issue is to resort to checkerboard and mesh-independency schemes. One-node hinges are caused by the same computational problems as checkerboard problem is, and it is indeed the mismodeling of a hinge by an artificially highly stiff one-node joint of two Q4 elements. Some partial solutions may come from the use of higher order elements plus a local stress constraint, the use of filtering methods, perimeter constraints or gradient control constraints, or the use of the MOLE constraint or the checkerboard constraint; with the latter being the most effective along with the most recently proposed nodal variable method. Also a post-processing work can be reasonable [47].

From the point of view of the free AM, hinged regions are still risky areas owing to their geometric shape. Being round shaped there will be points with undesirably sloped tangents (see Fig. 5) that may be in need of sacrificial support material, what yields a compromise between performance and support free additive manufacturing. If a totally self-supported topology is desired, performance may be harmed and vice versa. This is originated by the conversion of hinges to stiffer parts, sacrificing flexibility and minimizing the output motion when the overhang constraint is tightened.

For the sake of a support free additive manufacturing and an adequate output motion range, the design process must result in a self-supported and totally functional distributed compliant mechanism. The goal then is to seek free AM but not at the expense of practical performance. Therefore, in case of synthesis of mechanisms, there may be some cases where it is more advisable to limit the need for scaffold structures to the hinged areas only, rather that eliminating them. This will lead to the goal in mind and is possible due to the control parameter proposed.

In the following lines the effect of the control parameter over the hinges is introduced. The intention is to vary the values of that parameter from a loose value to a tight value. When the defined value is loose and lower than the natural overhang rate of the part, the resulting geometry equals the non-constrained optimized material lay out, and it is not until that natural rate is overcome that the final topology starts to differ from the previous and down-facing boundaries' slopes are corrected causing changes in the rest of the geometry. While an appropriate $\phi_0$ is used, the algorithm gives preference to performance rather than to the total elimination of the scaffold structures, with the enclosed advantage of keeping the balance between performance and manufacturability. In such cases, a correct description of hinged areas is ensured while the rest of the contours are improved according to the established threshold overhang angle and the value of the control parameter.

On the other hand, when an over restrictive value is set for the control parameter, the algorithm is too severe with the topology and not only corrects the boundary slopes but also modifies the hinges. This leads to topologies where manufacturability outweighs performance and the output motion range may be penalized (see Fig. 6).

Fig. 6 shows five different results, one for non-constrained topology and four results for a 45° constraint with different control parameter values. The evolution of the hinge through the different control parameters shows how the natural hinge shape degenerates into a more lineal and continuum bar shape for tighter values, a behavior that implies a loss of performance. Note however, that the upper boundary of that hinge still presents the typical reduction of the section while the down facing boundary becomes a totally straight line. Fig. 7 shows the idea behind the reduction of the support material volume for these previous cases.

At this point, it gets clear that for some designs there may be a compromise between support free additive manufacturing and performance. According to the examples shown, an increase of the control parameter to very tight values provokes such degeneration of the hinges that affects the mechanical performance of the mechanism. Although for the simplest compliant mechanisms this loss may not be very significant, it is for the more complex compliant mechanisms with a greater amount of hinges. Therefore, in such cases, it is advisable not to eliminate the scaffold structures but to limit them to the hinged areas only.

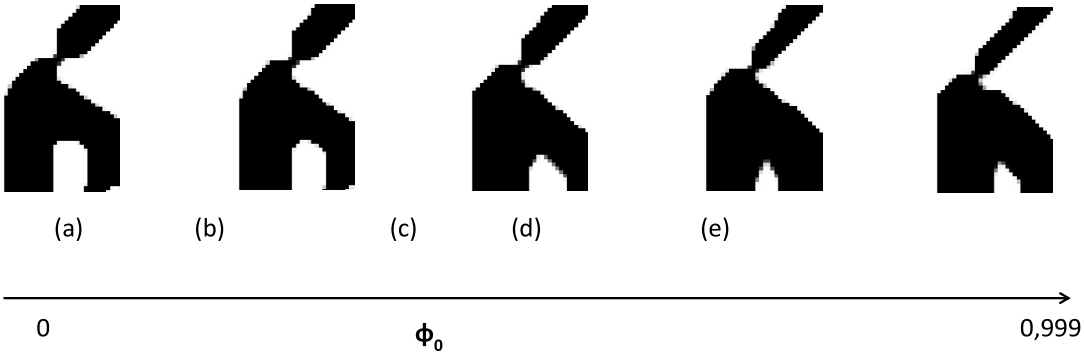


**Fig. 6.** Evolution of the hinges for different control parameters. (a) unrestricted, (b) $\phi_0 = 0.98$, (c) $\phi_0 = 0.99$, (d) $\phi_0 = 0.993$ and (e) $\phi_0 = 0.996$.

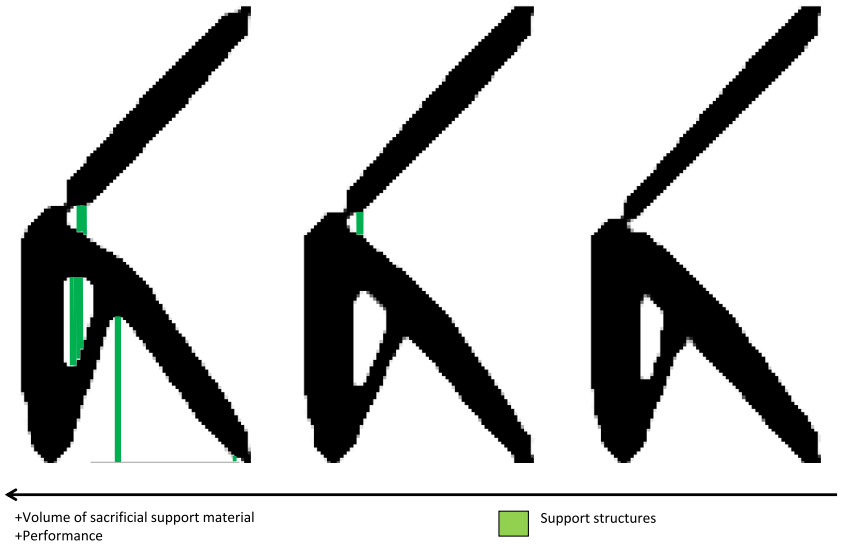


**Fig. 7.** Reduction of the support material volume. $\phi_0 = 0$, $\phi_0 = 0.99$ and $\phi_0 = 0.996$ respectively.

This strategy yields to well-shaped hinges and the performance is very close to the one of the non-constrained topology. It has also proven to lead to balanced designs where functional requirements are properly achieved as well as the free additive manufacturability is enhanced. In addition, minimum amount of sacrificial support material is ensured along with a minimization of post-processing needs.

Fig. 8 shows the real 3D printing results of the $\phi_0 = 0$ and $\phi_0 = 0.99$ cases presented in Fig. 6. The inverter has been built in a Fused Deposition Modeling (FDM) machine. This machine introduces support material in a very conservative way, so for a clear view of the correction of the overhang angles, the surplus of support material has been cleaned. This is fair since more modern AM machines introduce support material more wisely. The results in Fig. 8 demonstrate that while the unrestricted design requires some support material under the hinge, in the hole of the bracket and under the corner of the down-facing contour, in the constrained design the support structures are reduced to the hinge only. This proves that a flexible overhang constraint is of great use when a compromise between 3D printability and performance exists.

Gathering all the previous information, the introduction of the $\phi_0$ parameter is very useful in the optimum design of self-supported compliant mechanisms, providing an effective tool to control and minimize scaffold structures, while the functionality of the mechanism is encouraged.

## 6. Numerical examples

This chapter is reserved to benchmark examples and real application of the algorithm. Examples with different growing directions and several control parameters are shown for inverter and gripper mechanisms. Note that the best way to manufacture the mentioned mechanisms is by placing them horizontally inside the AM machine, with a vertical growing direction and building them as extruded 2D parts. In such case, there will be no need for support structures. However, this work aims to focus on the analysis of other growing directions as a preliminary step towards expansion of the algorithm to 3D domains. Finally, note that the values defined for the filter radius are slightly higher than the usual values. Although the proposed overhang constraint is global, the mask analyzes the contours locally, thus, it makes indispensable to resort to filter radiuses slightly greater than the typical values in order to avoid local solutions to the overhang constraint. The element-radius ratio used in the results has demonstrated to yield appropriate results.

### 6.1. Inverter mechanism

An inverter is a mechanism that converts an input force applied at the input port, into an opposite output displacement at the output port. This very first example is used to demonstrate the capacities of the algorithm as well as the influence of the growing direction. The design domain is rectangle with a width $W$ and

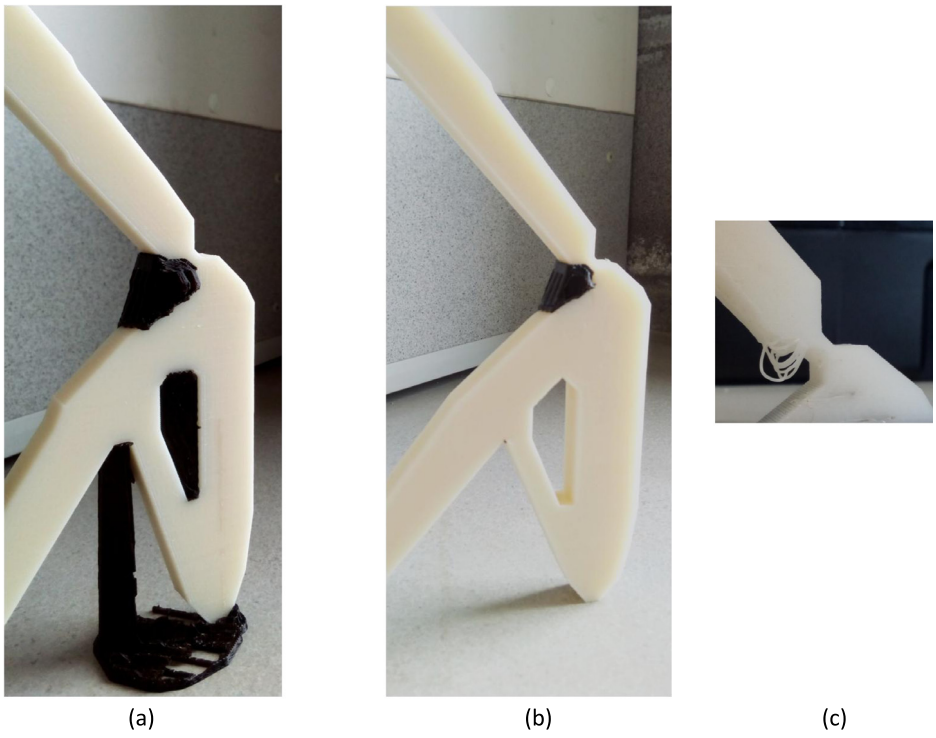


**Fig. 8.** Reduction of the support material required for printing a vertically positioned inverter mechanisms. (a) No restricted design. (b) Design restricted with a 45° overhang constraint and $\phi_0 = 0.99$. (c) Detail of a hinge built with no support material (failed printing due to the generation of dross).

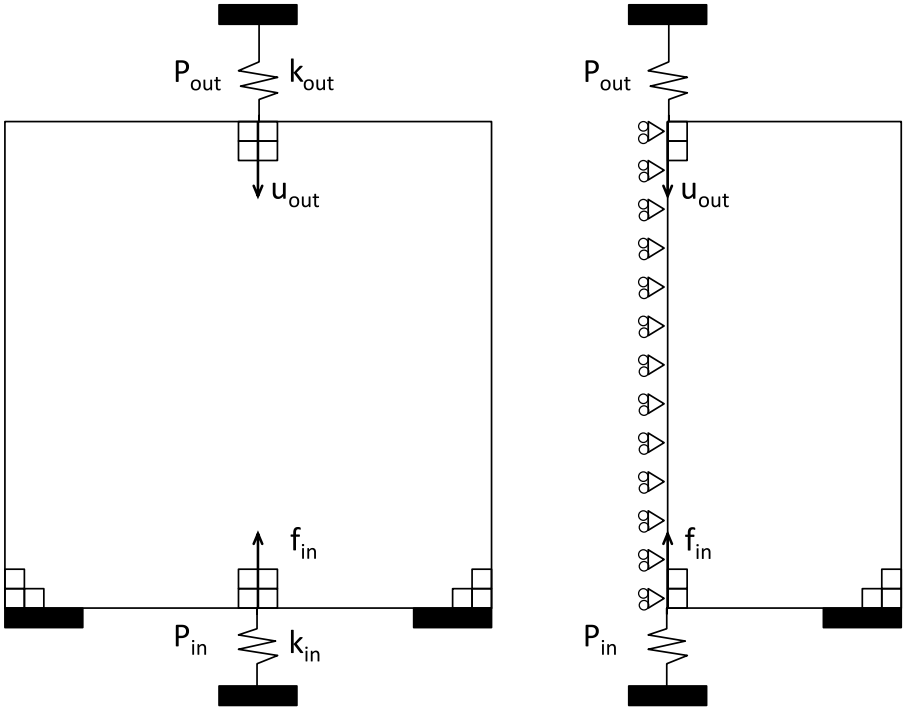


**Fig. 9.** Design domain for an inverter mechanism.

a height $H = W$. The input port ($P_{in}$), where the vertical input force $f_{in}$ is applied, is located in the middle node of the lower boundary; and the restricted degrees of freedom are placed at the sides of the lower face. The domain is discretized with $140 \times 140$ square elements, with edge length of 1.0 mm. The objective volume fraction is set to $V^* = 0.3$, the ratio of admissible contours in the overhang constraint is varied for values ranging from $\phi_0 = 0.98$–$0.996$, and the considered threshold angle is 45°. The filter radius is set to $r_{min} = 5.5$ mm, the Heaviside projection threshold to $T_r = 0.5$ and a vertical growing direction is considered. For the sake of simplicity, symmetry is considered as shown in Fig. 9.

Fig. 10 shows the result for the different control parameters and a plot of the values of Eq. (5) for the same results, where red color indicates unsupported contours. All the presented results have been obtained starting new optimizations processes. Fig. 10(a) stands for $\phi_0 = 0$ or non-constrained problem, which

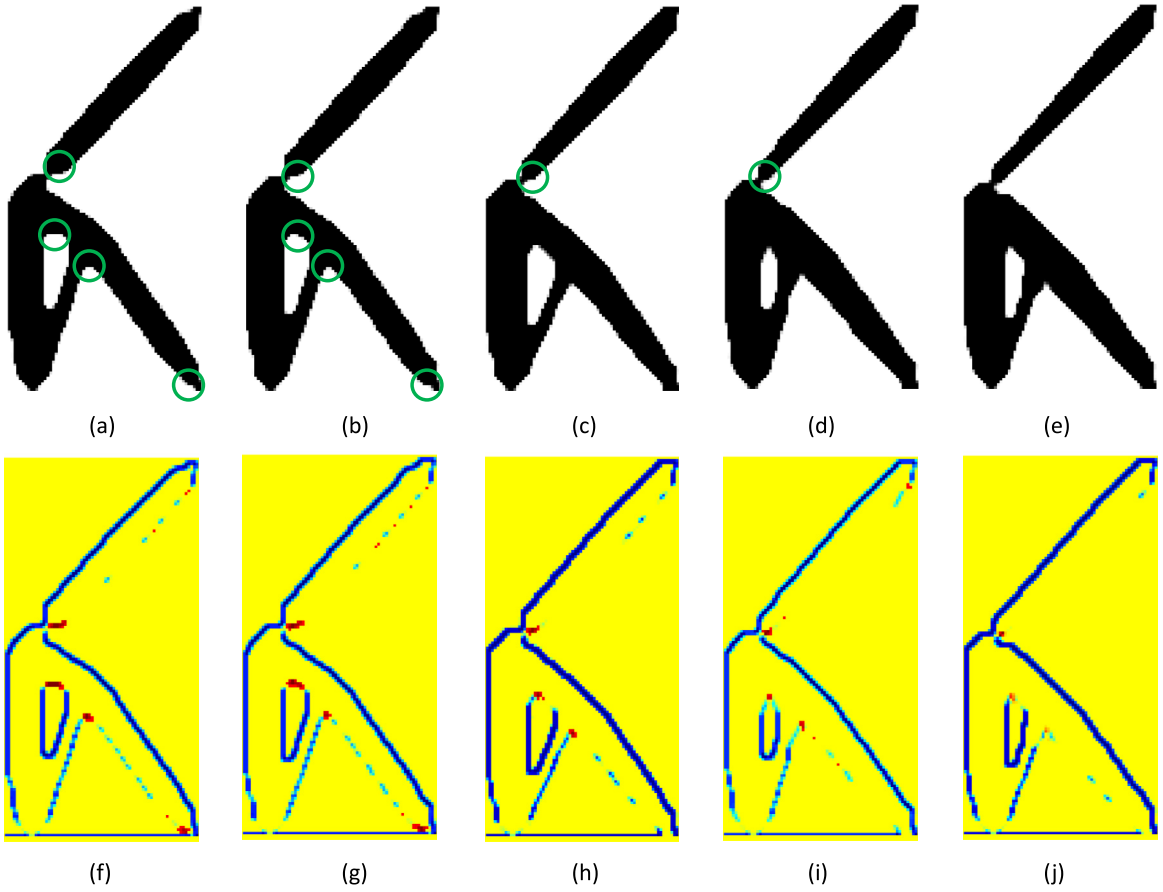


**Fig. 10.** (a)(f) non-constrained, $u_{out} = 0{,}3669$ mm. (b)(g) 45°, $\phi_0 = 0.98$, $u_{out} = 0{,}3666$ mm. (c)(h) 45° and $\phi_0 = 0.99$, $u_{out} = 0{,}3662$ mm. (d)(i) 45° and $\phi_0 = 0.995$, $u_{out} = 0{,}3645$ mm. (e)(j) 45° and $\phi_0 = 0.996$, $u_{out} = 0{,}3624$ mm . (For interpretation of the references to color in this figure legend, the reader is referred to the web version of this article.)

shows the natural overhang ratio of the structure, in this case $\phi_{0natural} = 0.974$. Its value denotes the amount of self-supported contours present in the non-constrained domain. In the second row of the figure it is appreciable that the number of red areas, as well as their length, is reduced as $\phi_0$ is tightened. Note that for the tightest control parameters, the upper corners or intersection of the down facing boundaries are sharpened and reduced to a single element. In terms of performance, the output displacement follows a downward trend as the control parameter is tightened.

Being round shaped, hinges have under-inclined tangents that make the introduction of sacrificial support material a must. Note however that although the control parameter gets tighter, the last area to be corrected is the hinge. This confirms the previous statement, which said that for the lower control parameter values the algorithm gives priority to boundaries and avoids correcting hinges, which is very advantageous regarding performance. Fig. 11 shows the convergence history of the result obtained in Fig. 10(c), where some intermediate results can also be observed, as well a detailed evolution of the change parameter, defined as the absolute value of the variation of the design variable in two consecutive iterations.

The problem takes 214 iterations, even so, the change parameter stays almost steady from iteration 109. It is because of the continuation scheme and the severe convergence criterion that the problem keeps evolving. Once the continuation scheme is over, it only takes 14 iterations to converge.

For this same topology and for the sake of exploring the capacities of the algorithm, a different growing direction or different part orientation is studied. Now the mechanism is supported over one of its sides (see Fig. 12). In such case, there are three possibilities to define the initial design domain. The designer can choose to either consider the whole domain or take advantage of the symmetry of the design domain and separately consider the upper or the lower part of the mechanism. Each of the possibilities will result in a different solution to the same problem, however, for the sake of maintaining symmetry and restrict the displacement at the output port to perfectly horizontal displacement; only optimization of the separated upper and lower parts is considered with the corresponding assembly process.

Fig. 13 shows the results for the same problem according to how the initial domain is chosen. For the proposed growing direction, the boundaries to be corrected are inverted, which occasions a rupture on the symmetry creating different upper and lower parts. Therefore, if the complete domain is considered, a non-symmetric result is evident, and in order to ensure that the output displacement is totally horizontal, an extra constraint would be needed. It is for that reason that such initial design domain will not be considered.

If symmetry is applied, the result also varies depending on the part chosen. For the upper side, the result is given in Fig. 13(b) where one can see how the boundaries are corrected to slopes of 45°. The hole formed by the bracket is corrected to a rhombic shape in order to lead to a proper inclination of the left upper member, and the lower left and right corners are given more material and horizontally enlarged in order to make easier the correction of the interior triangle. This triangle is also given greater sharpness, which yields a smaller curvature radio at the hinge, eliminating the need for scaffold structures and enhancing the proper printing

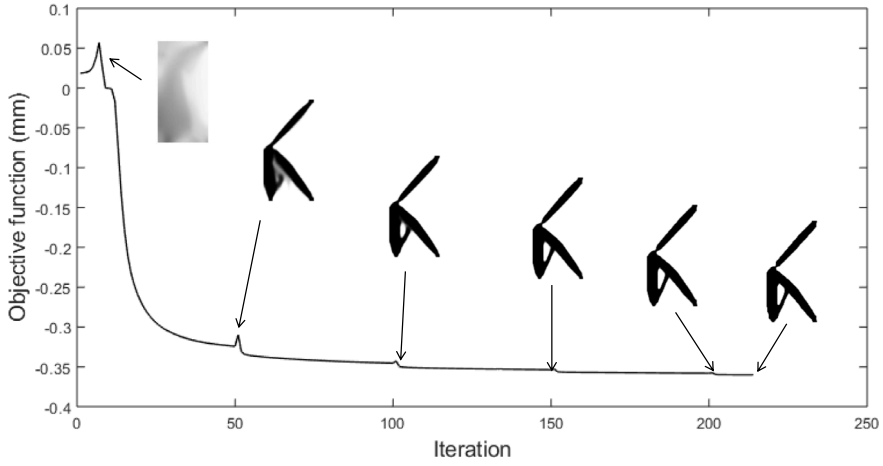


**Fig. 11.** Convergence history of the result (c) in Fig. 10.

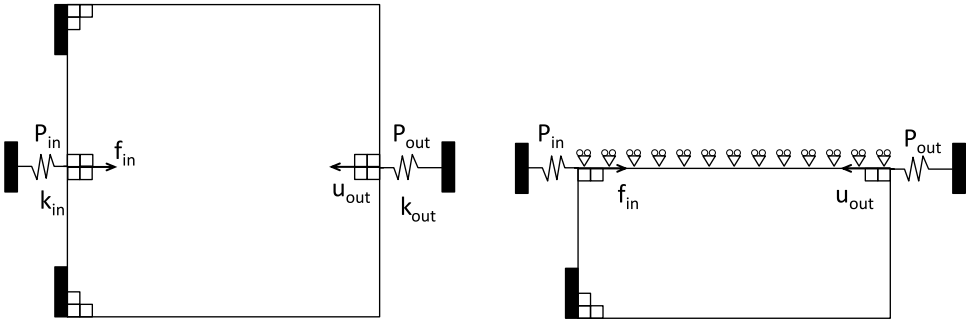


**Fig. 12.** Different possibilities for initial design domain of an inverter mechanism.


**Fig. 13.** The corresponding results for a 45° overhang constraint: (a) non-constrained whole mechanism, (b) upper symmetric side ($\phi_0 = 0.97$), $u_{out} = 0.3624$ mm and (c) lower symmetric side ($\phi_0 = 0.99$), $u_{out} = 0.3333$ mm.

of that area. If the lower side is considered, Fig. 13(c), the more appreciable effects are the conversion of the single bracket into two separate brackets and the pushing of the material on the left down size to the base. Note also that the hinge is stiffer order to enable free AM of the part. The rest of the down-facing contours are corrected to 45° slopes.

For this last building direction, if symmetry is desired in the final topology, manufacturing pairs of upper or lower parts is an option, however, an assembly process will be needed (see Fig. 14).

Fig. 15 compares different possible configurations for a 45° constraint and the displacement of the output port for each is compared to the non-constrained geometry.

The later results show that, for the case of the inverter, if a free additive manufacturing is sought, the best orientation to manufacture the mechanism, among the proposed above and excluding the horizontal positioning, is the vertical orientation. Compared to the non-constrained topology ($u_{out} = 0.3669$ mm) the output response of the self-supported topology ($u_{out} = 0.3662$ mm), which corresponds to the result displayed in Fig. 10(c), only drops by 0.19%, while with the strategy of assembling two lower or two upper parts it drops by %9.15 and %1.226 respectively. Then, it is possible to conclude that the growing direction severely influences the output response, and in case of the inverter the most adequate

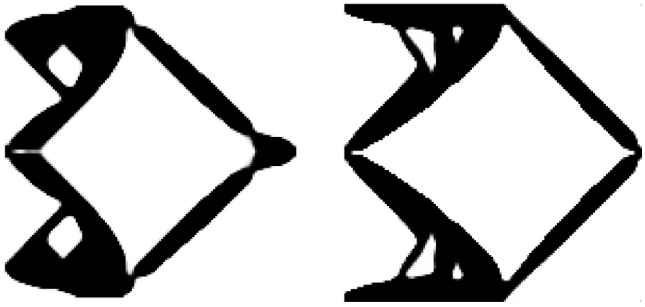

**Fig. 14.** Assembly of parts.

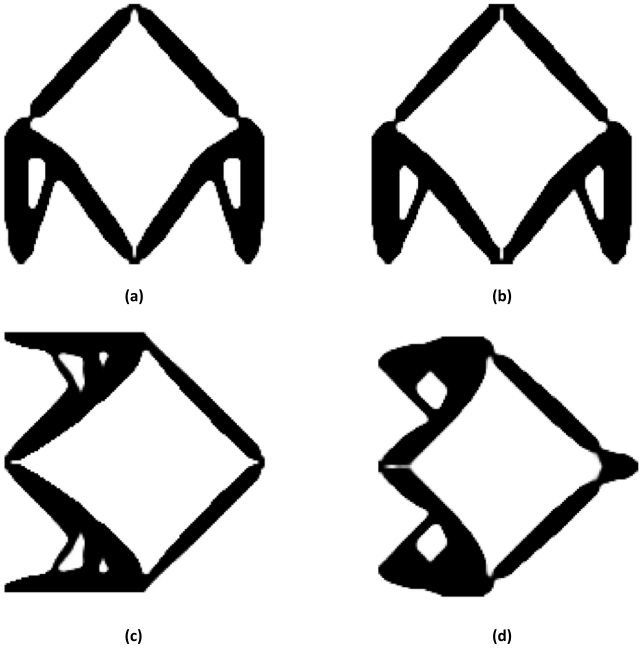


**Fig. 15.** Comparison of output topologies for different design-manufacturing strategies and the value of the output displacements: (a) unconstrained complete inverter, (b) 45° constrained complete inverter, (c) two lower part assembly and (d) two upper part assembly.

strategy is the vertical positioning with a vertical growing direction, as without the need for any assembly process, the output response is optimized. However, for any defined growing direction and positioning of the mechanism, the algorithm demonstrates a full capacity for controlling and correcting the overhang angle of the members.

### 6.2. Gripper mechanism

The gripper mechanism described in Fig. 16 converts a force, applied at the input port, into an output displacement at the two output ports in an orthogonal direction to the force vector. For this problem, the design domain is a rectangle of width $W$ and a height $H = W$. The input port ($P_{in}$), where the vertical input force $f_{in}$ is applied, is located in the middle node of the lower boundary; and the restricted degrees of freedom are placed at the sides of the lower boundary. The domain is discretized with $140 \times 140$ square elements, with edge length of 1.0 mm. The objective volume fraction is $V^* = 0.3$, the filter radius is $r_{min} = 5.5$ mm, the Heaviside projection threshold is set to $T_r = 0.5$ and the growing direction is vertical. For the sake of studying the capacity to deal with different angle restrictions, different minimum member inclination angles will be used.

Inside the initial design domain of a gripper there is a symmetric void space that forms the tweezers placed in the upper side with two active columns of solid elements that are the boundaries of the tweezers. Unlike in the inverter, in a gripper there are two output ports, symmetric to the vertical axis, named $P_{\text{out}}{}^1$ and $P_{\text{out}}{}^2$ respectively.

Due to the functionality of the gripper, if the goal is to eliminate the scaffold structures, the positioning of the mechanism lying over any of its symmetrical sides must be avoided, as the boundaries representing the jaws are fixed and horizontal for that position. Therefore, the approach to this design problem is made in vertical position.

Fig. 17 shows the results of the symmetric gripper, for (a) non-penalized, (b) 45° limit angle and (c) 60° limit angle.

The results show that while in the non-constrained problem the topology presents a geometry with 3 holes, for the 45° and 60° overhang angle constraints, the number of holes is lowered by 1 (2 holes). This produces more compact tweezers and allows the problem to form the most adequate boundary slopes at the holes. With respect to the hinges, there is a clear adaptation effect depending on the value of the minimum allowable inclination angle. In Fig. 17(d) the upper side of the non-constrained hinge has a left tangent with a mean inclination lower than 45°, that is the theoretically accepted standard limit angle, and a right hand tangent very close to the horizontal. Both areas will be in need of the introduction of support structures to avoid collapsing. As shown in Fig. 16(e) and (f), the under-inclination of these tangents is corrected when the overhang restriction is considered. For each case the slopes of the tangents are corrected according to the limit angle, in these cases 45° and 60°, respectively. The rest of the contours are also corrected according to that angle, demonstrating the effectiveness of the algorithm. For the results shown in Fig. 17 the corresponding values of the objective functions are 0.3445 mm, 0.3314 mm and 0.3155 mm, clearly showing that the more severe the angle constraint is, the more penalized the output displacement will be.

The nature of the hinges is also modified for the 60° constraint. Here the single hinge seen in Fig. 17(a) and (b) is converted into a double hinge separated in the clumped member and the member sprouting from the input port. This new hinge configuration is due to the value of 60° for the overhang angle constraint. Being more restrictive than a 45° overhang angle, the value of 60° forces the topology optimization problem to form such hinge geometry, which can be more efficient with respect to the additive manufacturing process.

The proposed method not only allows the designer to define different overhang angles, but also allows him to define different control parameters. The responses to different values of this parameter for the gripper are shown in Fig. 18.

From Fig. 18 it can be directly concluded that the tighter the control parameter is, the more differs the final topology form the material lay out obtained for the non-constrained problem. The evolution of the geometry shows a tendency to erase one of the holes in the tweezers, going from 3 to 2. These holes are rotated and positioned so that one of their vertices occupies the highest part, thus, allowing the formation of controlled down-facing boundaries. For greater values of $\phi_0$ the slopes of the tangents at the hinges are corrected too. This latter effect is appreciated when Fig. 18(c), (d) and (e) are compared; demonstrating again that the algorithm is able to control the inclination of the members according to the defined minimum allowable overhang inclination angle and the control parameter.

Similarly, the gripper can also be rotated and manufactured upside down. The result, although similar to the ones obtained in the previous positioning, the holes are sharpened the other way around, as Fig. 19 shows. Other differences are, the shape of the input port and the shape of the hinge. For the new growing direction the unsupported contours are inverted, thus, the hinge shows the opposite configuration to the one in the result of Fig. 18.

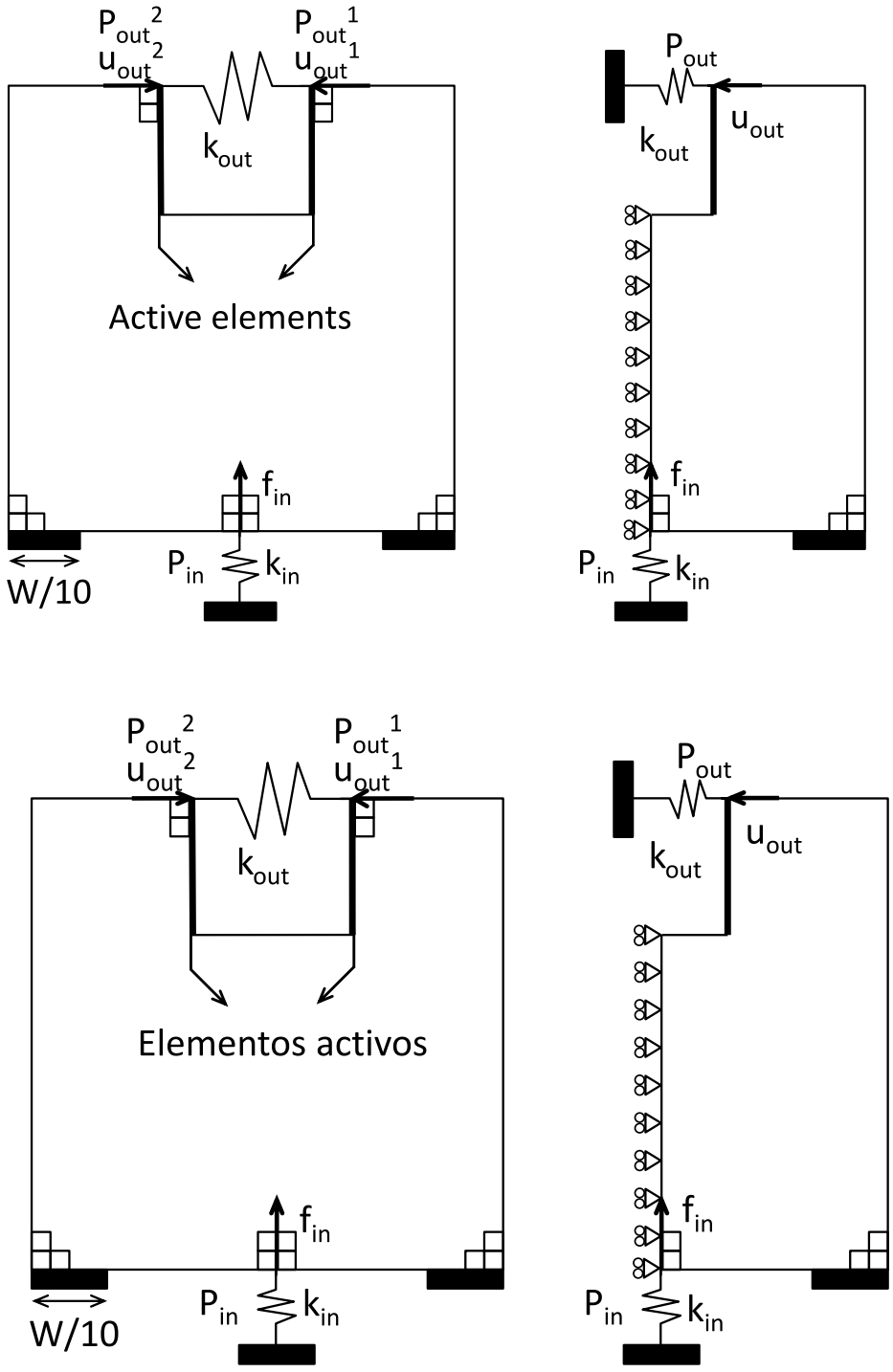


**Fig. 16.** Design domain for a gripper mechanism.

## 7. Conclusions

The early sections of this work mentioned the challenge of the design of optimal self-supporting compliant mechanisms, and the compromise there is when a designer seeks support free AM and an adequate level of output response all together. It is common knowledge that flexible mechanisms obtain their flexibility from hinges or flexural points distributed along the design domain and that the geometry of these pivots is a key factor for optimizing the output response. However, the optimal shape of a hinge is not very AM friendly, which implies that when an overhang constraint is introduced, the hinges will be completely reshaped. Nevertheless, the introduction of a control parameter proves to be very helpful balancing that effect according to the needs of the designer.

The proposed flexible overhang constraint allows either eliminating or minimizing the usage of sacrificial support material. Nevertheless, for a constraint of 45°, which is the most common for any AM process, we found that it is possible to obtain perfectly support free manufacturable geometries for the inverter and gripper cases where the performance is not significantly penalized.

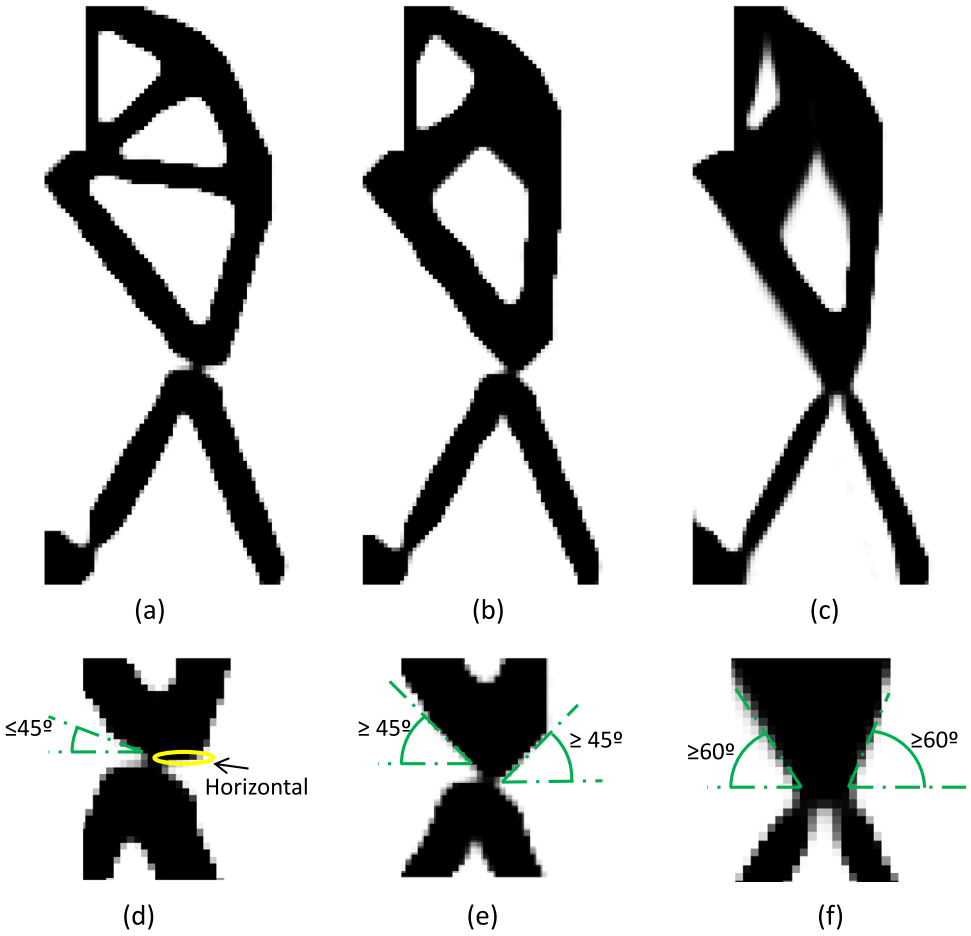


**Fig. 17.** Results for (a) non-constrained topology, (b) 45° constraint ($\phi_0 = 0.992$) and (c) 60° constraint ($\phi_0 = 0.970$). (d), (e) and (f): Evolution of the hinges.

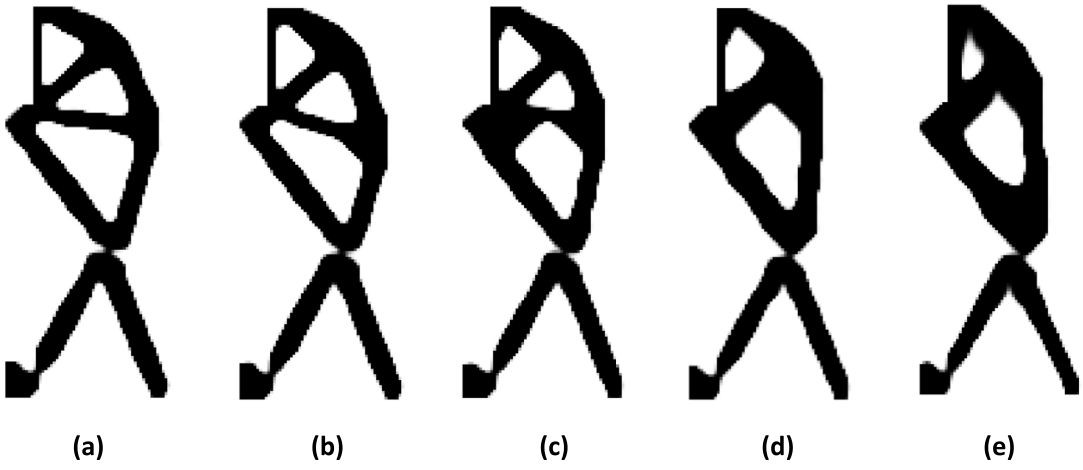


**Fig. 18.** Results of a gripper mechanism for a 45° minimum overhang angle and control parameters values of (a) $\phi_0 = 0/0.93$, (b) $\phi_0 = 0.96$, (c) $\phi_0 = 0.982$, (d) $\phi_0 = 0.992$ and (e) $\phi_0 = 0.998$.

In view of the results, it may be concluded that the method proposed in this paper is effective and practical when it comes to coupling the optimum topology design and additive manufacturing processes of compliant mechanisms, and so does extend the concept of "topology optimization for additive manufacturing" to the field of the compliant mechanisms. Future work will be to open this method to 3D mechanisms.

## Acknowledgments

This work was supported by The European Regional Development Fund (ERDF-FEDER) and the Ministry of Education and Science in Spain through the DPI2015-64863-R project (MINECO/FEDER-UE). The authors also wish to thank the Basque Government for financial assistance through IT919-16. The authors are

**Fig. 19.** The resulting self-supported design for the inverted compliant gripper, $\phi_0 = 0.995$ and $u_{out} = 0.3314$ mm.

beneficiary of the Predoctoral Program for the Training of Non-Doctor Researchers of the Department of Education of the Basque Government.

## References


[1] Sevak N, Mclaman C. Optimal synthesis of flexible link mechanisms with large static deflection. In: ASME, Vol. 83. 1974.

[2] Her I, Midha A. A compliance number concept for compliant mechanisms and type synthesis. J Mech Transm Autom Des 1987;109(3):348–55.

[3] Howell L, Midha A. A generalized loop-closure theory for the analysis and synthesis of compliant mechanisms. In: Proceecings of ASME, machine elements and machine dynamics. 1994, p. 491–500.

[4] Howell L, Midha A. A method for the design of compliant mechanisms with small-length flexural pivots. Trans ASME J Mech Des 1994;116(1):280–90.

[5] Bendsøe MP. Optimal shape design as a material distribution problem. Struct Optim 1989;1(4):193–202.

[6] Zhou M, Rozvany GIN. The COC algorithm, Part II: Topological, geometrical and generalized shape optimization. Comput Methods Appl Mech Engrg 1991;89(1–3):309–36.

[7] Stolpe M, Svanberg K. An alternative interpolation scheme for minimum compliance topology optimization. Struct Multidiscip Optim 2001;116–24.

[8] Bendsøe MP, Kikuchi N. Generating optimal topologies in structural design using a homogenization method. Comput Methods Appl Mech Engrg 1988;71(2):197–224.

[9] Xie Y, Steven G. Shape and lay out optimization via an evolutionary procedure. In: International conference on computational engineering science. 1992, p. 471.

[10] Yang XY, Xei YM, Steven GP, Querin OM. Bidirectional evolutionary method for stiffness optimization. AIAA J 1999;37(11):1483–8.

[11] Ansola R, Veguería E, Canales J, Tárrago JA. A simple evolutionary topology optimization procedure for compliant mechanism design. Finite Elem Anal Des 2007;44(1–2):53–62.

[12] Rozvany G, Querin OM. Theoretical foundations of sequential element rejections and admissions (SERA) methods and their computational implementation in topology optimization. In: 9th AIAA/ISSMO symposium on multidisciplinary analysis and optimization. American Institute of Aeronautics and Astronautics; 2002.

[13] Allaire G, Jouve F, Toader AM. Structural optimization using sensitivity analysis and a level-set method, 194 (1) 2004.

[14] Sokolowski J, Zochowski A. On the topological derivative in shape optimization. SIAM J Control Optim 1999;37(4):1251–72.

[15] Zhang W, Yuan J, Zhang J, Guo X. A new topology optimization approach based on Moving Morphable Components (MMC) and the ersatz material model. Struct Multidiscip Optim 2016;53(6):1243–60.

[16] Doubrovski Z, Verlinden J, Geraedts J. Optimal design for additive manufacturing: opportunities and challenges. In: ASME 2011 internationa design engineering technical conferences and computers and information in engineering conference. 2011, p. 635–46.

[17] Chang K-H, Tang P-S. Integration of design and manufacturing for structural shape optimization. Adv Eng Softw 2001;32(7):555–67.

[18] Leary M, Babaee M, Brandt M, Subic A. Feasible build orientations for self-supporting fused deposition manufacture: A novel approach to space-filling tesselated geometries. Adv Mater Res 2013;633:148–68.

[19] Thomas D. The development of design rules for selective laser melting. University of Wales Institute; 2009.

[20] Leary M, Merli L, Torti F, Mazur M, Brandt M. Optimal topology for additive manufacture: A method for enabling additive manufacture of support-free optimal structures. Mater Des 2014;63:678–90.

[21] Morgan HD, Cherry JA, Jonnalagadda S, Ewing D, Sienz J. Part orientation optimisation for the additive layer manufacture of metal components. Int J Adv Manuf Technol 2016;86(5–8):1689.

[22] Vanek J, Galicia JAG, Benes B. Clever support: Efficient support structure generation for digital fabrication. Comput Graph Forum 2014;33(5):117–25.

[23] Calignano F. Design optimization of supports for overhanging structures in aluminum and titanium alloys by selective laser melting. Mater Des 2014;64:203–13.

[24] Mirzendehdel AM, Suresh K. Support structure constrained topology optimization for additive manufacturing. CAD Comput Aided Des 2016;81:1–13.

[25] Hu K, Jin S, Wang CCL. Support slimming for single material based additive manufacturing. CAD Comput Aided Des 2015;65:1–10.

[26] Brackett D, Ashcroft I, Hague R. Topology optimization for additive manufacturing. In: Solid freeform fabrication symposium. 2011, p. 348–62.

[27] Gaynor AT, Guest JK. Topology optimization considering overhang constraints: Eliminating sacrificial support material in additive manufacturing through design. Struct Multidiscip Optim 2016;54(5):1157–72.

[28] Langelaar M. An additive manufacturing filter for topology optimization of print-ready designs. Struct Multidiscip Optim 2017;55(3):871–83.

[29] Langelaar M. Topology optimization of 3D self-supporting structures for additive manufacturing. Addit Manuf 2016;12:60–70.

[30] Qian X. Undercut and overhang angle control in topology optimization: A density gradient based integral approach. Internat J Numer Methods Engrg 2017;111(3):247–72.

[31] Serphos MR. Incorporating AM-specific Manufacturing Constraints into Topology Optimization PRESENTATION, 2014.

[32] Guo X, Zhou J, Zhang W, Du Z, Liu C, Liu Y. Self-supporting structure design in additive manufacturing through explicit topology optimization. Comput Methods Appl Mech Engrg 2017;323:27–63.

[33] Svanberg K. The method of moving asymptotes. A new method for structural optimization. Internat J Numer Methods Engrg 1987;24(2):359–73.

[34] Mokrzycki W, S M. Using SUSAN method to color contour producing. 2009.

[35] Fynbo J, Rasmussen J, Olhoff N. A directional topology optimisation method. In: Proceedings of the 4th world congress of structural and multidisciplinary optimization, WCSMO-4. 2001.

[36] Walter N, Aubreton O, Laligant O. Susan 3D characterization for manufactured cylinder edge detection. In: International conference on quality control by artificial vision. 2009.

[37] Walter N, Aubreton O, Fougerolle YD, Laligant O. SUSAN 3D operator principal saliency degrees and directions extraction and a brief study on the robustness to noise. In: 2009 16th IEEE international conference on image processing (ICIP). 2009, p. 3529–32.

[38] Garaigordobil A, Ansola R, Veguería E. Discretización del dominio de diseño en problemas de Optimización de Topologıa con Restricciones de Fabricación Aditiva. In: CMN 2017 congress on numerical methods in engineering, no. July. 2017, p. 1412–26.

[39] Díaz A, Sigmund O. Checkerboard patterns in layout optimization. Struct Optim 1995;10(1):40–5.

[40] Jog CS, Haber RB. Stability of finite element models for distributed-parameter optimization and topology design. Comput Methods Appl Mech Engrg 1996;130(95):203–26.

[41] Haber RB, Jog CS, Bendsoe MP. A new approach to variable-topology shape design using a constraint on perimeter. Struct Optim 1996;11:1–12.

[42] Sigmund O, Petersson J. Numerical instabilities in topology optimization: A survey on procedures dealing with checkerboards, mesh-dependencies and local minima. Struct Optim 1998;16(1):68–75.

[43] Bourdin B. Filters in topology optimization. Internat J Numer Methods Engrg 2001;50(9):2143–58.

[44] Guest JK, Prévost JH, Belytschko T. Achieving minimum length scale in topology optimization using nodal design variables and projection functions. Internat J Numer Methods Engrg 2004;61(2):238–54.

[45] Wang F, Lazarov BS, Sigmund O. On projection methods, convergence and robust formulations in topology optimization. Struct Multidiscip Optim 2011;43(6):767–84.

[46] Guest JK, Asadpoure A, Ha SH. Eliminating beta-continuation from Heaviside projection and density filter algorithms. Struct Multidiscip Optim 2011;44(4):443–53.

[47] Bendsøe MP, Sigmund O. Topology optimization: Theory, methods, and applications, Vol.724. 2nd ed.. 2003.
[48] Paros J, Weisbord L. How to design flexural hinges. Mach Des 1965;37:151–6.
[49] Alonso C, Querin OM, Ansola R. A sequential element rejection and admission (SERA) method for compliant mechanisms design. Struct Multidiscip Optim 2013;47(6):795–807.
[50] Saxena A, Ananthasuresh GK. Topology optimization of compliant mechanisms with strength considerations. Mech Struct Mach 2001;29(2):199–221.
[51] Rahmatalla S, Swan CC. Sparse monolithic compliant mechanisms using continuum structural topology optimization. Internat J Numer Methods Engrg 2005;62(12):1579–605.